Correlated Flux Densities From VLBI Observations With the DSN

R. F. Coker
Tracking Systems and Applications Section

Correlated flux densities of extragalactic radio sources in the very long baseline interferometry (VLBI) astrometric catalog are required for the VLBI tracking of Galileo, Mars Observer, and future missions. A system to produce correlated and total flux density catalogs has been developed to meet these requirements. A correlated flux density catalog of 274 sources, accurate to about 20 percent, has been derived from more than 5000 DSN VLBI observations at 2.3 GHz (S-band) and 8.4 GHz (X-band) using 43 VLBI radio reference frame experiments during the period 1989–1992. Various consistency checks have been carried out to ensure the accuracy of the correlated flux densities. All observations were made on the California–Spain and California–Australia DSN baselines using the Mark III wideband data acquisition system. A total flux density catalog, accurate to about 20 percent, with data on 150 sources, has also been created. Together, these catalogs can be used to predict source strengths to assist in the scheduling of VLBI tracking passes. In addition, for those sources with sufficient observations, a rough estimate of source structure parameters can be made.

I. The Need for Correlated Flux Densities

An astrometric catalog of compact extragalactic radio sources (generically referred to as quasars) is produced and maintained using VLBI observations with the DSN [1]. The primary purpose of this catalog is to provide a reference frame for angular tracking measurements of interplanetary spacecraft. Such tracking requires a catalog with a moderately high angular density of observable reference quasars along a spacecraft trajectory. In the standard tracking mode, it is generally desirable to have at least one observable reference quasar within about 10 deg of the spacecraft position at all times, since errors in the interferometric delay measurements grow with quasar–spacecraft separation.[1] In an alternate tracking mode, several quasars within a 30- to 50-deg field are observed to form a "local reference frame" in which the position of the spacecraft can be measured with extremely high accuracy [2].

Navigational scheduling requires a priori knowledge regarding which antennas are needed to observe, with an SNR adequate for detection, a specific quasar on a specific

[1] J. B. Thomas, "An Error Analysis for Galileo Angular Position Measurements with the Block II ΔDOR System," JPL Engineering Memorandum 335-26 (internal document), Jet Propulsion Laboratory, Pasadena, California, November 11, 1981.

baseline. Nominally, the correlated flux density detection limits, using the DSN's operational 250-kHz bandwidth navigation VLBI system (the Block I system), are about 0.2 Jy (1 Jy is 10^{-26} W/m^2/Hz) for two 70-m antennas, 0.4 Jy for one 70-m and one 34-m antenna, and 0.8 Jy for two 34-m antennas.[2] These limits apply at 8.4 GHz (X-band); at 2.3 GHz (S-band) the limits are somewhat higher at 0.2, 0.5, and 1.0 Jy, respectively, due to higher system temperatures. Since the correlated flux density of a given quasar can change from month to month by as much as 50 percent in extreme cases (especially at higher observing frequencies, such as X-band) [3], it is necessary to make correlated flux density estimates a routine part of reference frame data processing. A method has been developed which easily and quickly produces a correlated and total flux density catalog that is accurate enough (~20 percent) to determine which antenna pairs will be able to detect specified reference sources.

Flux density monitoring will also assist in quickly identifying sources that are inappropriate for reference frame determinations due to large variations in correlated flux density with baseline angle (as a result of extensive structure). It will also provide valuable time and source structure variability information. Prior to this work, no method existed for producing correlated flux density data from DSN Mark III Block II observations (see [4] for Mark III system details). In addition, the production of correlated flux density data from DSN Mark II observations was tedious and the results were often highly uncertain.[3] The new flux density estimates (with a detection limit of approximately 30 mJy), as well as the developed methodology, will be useful to anyone using the DSN to observe natural radio sources.

This article is organized in the following manner: Section II presents the expression for correlated flux density and gives details of the production and contents of the flux density catalogs. Section III describes the consistency checks and integrity tests carried out to verify the flux density results. The error budget is discussed in Section IV. Section V summarizes the results.

[2] J. S. Border, "An Error Analysis for Magellan Differential Delay Rate Measurements," JPL Engineering Memorandum 335-96 (internal document), Jet Propulsion Laboratory, Pasadena, California, February 23, 1987.

[3] I. Chen and J. S. Ulvestad, "Determination of Correlated Flux Densities from Mark II VLBI Experiments," JPL Interoffice Memorandum 335.3-88-102 (internal document), Jet Propulsion Laboratory, Pasadena, California, September 22, 1988.

II. Estimating Correlated Flux Densities and Total Flux Densities

For a radio source with nonzero angular size, the correlated flux density (i.e., that measured with an interferometer) will always be less than the total flux density. Roughly speaking, the correlated flux density is the strength of that part of the source which is angularly small as compared with an interference fringe on the sky. The angular width of an interference fringe is λ/B, where λ is the observing wavelength and B is the projected length of the interferometer baseline in the plane perpendicular to the source direction. The correlated flux density of a resolved source will vary as a function of baseline length and orientation because source structure is two-dimensional. In the absence of a complete, current description of the structure of a source, there is no way to specify a priori the source visibility (defined as the ratio of correlated flux density to total flux density) [5].

The correlated flux density, S_{cor}, of a source is given by[4]

$$S_{cor} = \frac{\sin(\rho\,\pi/2)}{b}\sqrt{\frac{T_{sys_1}T_{sys_2}}{G_1G_2}} \qquad (1)$$

where ρ is the correlation amplitude for data recorded with one-bit sampling, b is a normalization factor due to correlator and bandpass effects (with this definition, b for DSN Mark III data is greater than 1; see Section III.A for details), T_{sys_i} is the total on-source system temperature at station i in kelvins (K), and G_i is the antenna gain at station i in K/Jy [6]. In addition, the total flux density, S_{tot}, as measured by a single antenna with gain G, can be written as

$$S_{tot} = \frac{T_{on} - T_{off}}{G} = \frac{T_{ant}}{G} \qquad (2)$$

Here T_{on} and T_{off} are on-source and off-source system temperatures, respectively, and T_{ant} is the antenna temperature.

Using the new procedure reported here, correlated flux densities are obtained from DSN Mark III VLBI data that have been correlated at the JPL/CIT Block II correlator, with observable (e.g., delay and amplitude) extraction by

[4] R. F. Coker, "Mark III Correlated Flux Densities on the DSN," JPL Interoffice Memorandum, 335.6-91-028 (internal document), Jet Propulsion Laboratory, Pasadena, California, December 31, 1991.

the program FIT [7]. A master program takes the schedule file for the DSN antennas, correlation amplitudes, and observing frequencies from FIT, the measured system temperatures from antenna log files, and the modeled antenna gain, and produces a correlated flux density and a total flux density catalog. Details of this procedure are given below.

A. Amplitudes, Frequencies, and Hour Angle

The observing frequency and the correlation amplitude for each observation are read in from the FIT output file. The FIT data are assumed to be DSN Mark III Block II dual band (S- and X-bands), Mark III X-band only, or Mark II X-band only. One method of specifying baseline orientation is the interferometer hour angle (IHA) [6]; therefore, the correlated flux density of a resolved source will vary with the IHA. The source positions (right ascension and declination), observation times, and station locations are taken from the schedule file and used to calculate the IHA for each observation.

B. System Temperatures

System temperatures are obtained from strip-chart data files, data files produced by power meters, or from a mapping function using an estimated off-source zenith system temperature.

1. Strip charts. Strip-chart data files are lists of sources with system temperatures and error estimates read from strip charts. The independently measured zenith system temperature (recorded in the station logs) can be used to check for mistakes in the labeling, reading, or editing of the strip-chart file. In general, however, due to operator errors and instrument inaccuracies, strip-chart system temperature values remain unreliable. Also, the receiver used for strip-chart measurements is not the same receiver as that used for reference frame experiments. Therefore, other methods are preferred.

2. Power Meter Data. Power meter data are machine-readable total power values measured at the intermediate frequency expansion ports at a station. These time-tagged power readings are used to determine system temperature as a function of time.

For a given bandpass, system temperature is proportional to observed power [6]. Therefore, a single simultaneous power and system temperature measurement is adequate to convert the power readings to system temperatures. Using zenith system temperature and zenith power values that are in the header of each data file, the system temperature, T_{sys}, for a given observation is

$$T_{sys} = T_{zen} \frac{10^{(P/10)}}{10^{(P_{zen}/10)}} \tag{3}$$

where P is a power reading (in dBm) for that observation, P_{zen} is a power reading (in dBm) taken at zenith on cold sky, and T_{zen} (in K) is the zenith system temperature. There are usually about 40 power readings per 2- to 5-min observation; an average temperature is used for an observation's final system temperature. Errors are estimated from the scatter of the power data about a linear fit of the observation's power readings versus time, and the estimated error in P_{zen} and T_{zen}.

3. Modeling. If no system temperature data are available for a given frequency band and observing station, they are estimated using a temperature mapping function which relates the off-source system temperature at elevation angle *elev* to that at the zenith. An experimentally determined mapping function is used[5]

$$T_{sys} = A + N_1 \, e^{-N_2/(90^\circ - elev)} + \frac{B}{\sin(elev)} \tag{4}$$

where N_1 and N_2 depend on band and station, and *elev* is the elevation of the observation in degrees [8,9]. For stations without N_1 and N_2 values, a temperature version of the Chao mapping function is used [10].

If the total flux density of a source is known, the resulting antenna temperature is added to the modeled off-source system temperature. Antenna temperatures are usually less than 5 percent of the total system temperature, but for strong sources their contribution to the total system temperature is more significant.

4. Zenith System Temperatures. T_{zen} is calculated at the beginning of an experiment by taking a power reading of an ambient load and then of the sky; the difference, the Y factor (in dB), is a measurement of the receiver gain. Then T_{zen} is calculated

$$T_{zen} = \frac{T_{LNA} + T_{FO} + T_{amb}}{10^{(Y/10)}} \tag{5}$$

T_{amb} is the temperature of the ambient load. The noise temperatures used for the low-noise amplifier, T_{LNA}, and for the follow-on hardware (e.g., cables and waveguide),

[5] S. D. Slobin, *DSN Telecommunications Interfaces 34-Meter Antenna Subnets*, Document 810-5, Rev. D, vol. I, TCI-30, Jet Propulsion Laboratory, Pasadena, California, June 1, 1990.

T_{FO}, were incorrect before April 1991.[6] This introduced an error of a few K in T_{zen}. Formal precision measurement errors for T_{zen} appear small (~0.1 K), but the stability of T_{LNA}, T_{FO}, and T_{amb} values (as well as operator errors and weather effects) suggest that the overall accuracy of T_{zen}, as calculated above, is ~5 percent.[7,8]

The method for converting observed power to temperature, as described by Eqs. (3) and (5), implicitly assumes that for a given bandpass, power is directly proportional to the system temperature. For very large values of total power (corresponding to system temperatures of ~300 K), this assumption of detector linearity breaks down (at the 1- to 2-percent level).

C. Antenna Gains

The antenna gain for each station is modeled using experimentally determined functions; only a summary of the gain estimation procedure is given here (see [8] for details). The desired quantity is gain, G, in units of K/Jy (to use in Eq. (1)):

$$G = \frac{\eta\ Area}{2\ k} \tag{6}$$

where k is Boltzmann's constant, η is the antenna aperture efficiency, and $Area$ is the antenna's total physical collecting area. Variations in η across a given band are assumed to be negligible. The antenna aperture efficiency depends on the deformation of the antenna from its optimal shape, on weather conditions, and on the basic characteristics of the antenna surface. Thus, it can be written as

$$\eta = \eta_{max}\eta_{def}\eta_{atm} \tag{7}$$

where η_{max} is the aperture efficiency in a vacuum with no deviations from a perfectly shaped surface; η_{def} accounts for efficiency losses due to antenna gravitational deformation; and η_{atm} accounts for losses due to atmospheric attenuation. The value η_{max} is constant for a given antenna while η_{def} and η_{atm} depend on antenna elevation and weather conditions. The overall accuracy of the antenna gains modeled in this fashion (exclusive of antenna pointing effects; see Subsection III.C) is estimated at ~5 percent.

[6] Personal communication from T. Anderson, TDA Mission Support and DSN Operations Section, Jet Propulsion Laboratory, Pasadena, California, to C. Jacobs, member of technical staff, Tracking Systems and Applications Section, Jet Propulsion Laboratory, Pasadena, California, April 1, 1991.

[7] Slobin, op. cit.

[8] K. Clark and C. Cho, "Front-End Characteristics for NCB VLBI," JPL Interoffice Memorandum OEA.14/12.07.e.0, Jet Propulsion Laboratory, Pasadena, California, December 7, 1990.

III. Consistency Checks and Integrity Testing

A number of tests were carried out to verify the validity of the flux density catalogs. Since standard flux monitoring techniques (such as antenna nodding, repeated zenith calibrations, and standard source comparisons) are impractical for reference frame experiments due to time constraints, the internal and absolute accuracy of the DSN Mark III flux densities had to be determined in other ways.

A. Correlation Amplitudes and Their Normalization

The b-factor in Eq. (1) normalizes the correlation amplitude so that a signal with 100-percent correlation produces an amplitude of unity. Assuming identical bandpasses and a flat power spectrum and ignoring Doppler and polarization effects, one has, for some frequency ω [11],

$$b_\omega = a_1\ \frac{(BW_0)\ B^2}{D_N} \tag{8}$$

where

a_1 = 1.176 for a three-level lobe rotator, one path [6]

BW_0 = nominal or Nyquist bandwidth (2 MHz for a single Mark III channel)

B^2 = bandpass amplitude at ω

$D_N = \int_0^\infty B^2\ d\omega$

Note that the correction for single-bit quantization ($\approx 2/\pi$) is included in the expression for S_{cor} in Eq. (1).

The value B^2 is included in FIT's calculation of the correlation amplitude, ρ. This results in a b-factor that is independent of frequency. The value of B^2 was empirically calculated from over 200 Mark III and Mark II observations; the results, which agree reasonably well with theoretical bandpass shapes, are listed in Table 1. These values are used in FIT to weight the amplitude of each bin to produce one composite amplitude for each band. Also included in Table 1 are values for D_N. The value D_N is constant at the 1- to 2-percent level for any given correlator configuration (e.g., number of delay lags per channel). The resulting b-factor for DSN Mark III 8 lag data is 1.34.

Variable Doppler shifting due to Earth rotation causes the two station bandpasses to be mismatched by up to 20 kHz at X-band; this has been ignored. The frequencies of the local oscillators are not adjusted to correct for this Doppler shift. In addition, there will be some small changes in b due to mismatched bandpasses as a result of polarization effects (the actual size of this effect is unknown but DSN specifications suggest it is ~1 percent). These effects, combined with aliasing of frequencies above 2 MHz, correlation of neighboring bits due to oversampling, and incomplete sideband rejection imply that b will vary at the ~2-percent level. These effects, plus errors in modeling, give an estimated maximum error of approximately 5 percent in the b-factor.

Two errors in the standard data path were uncovered during this work. The first involved the fractional bit-shift (FBS) correction at the correlator. If the FBS correction is not done, the upper and lower 10 percent of the bandpass lose ~10 to 15 percent in amplitude [12]. This causes a composite loss in band amplitude of ~4 percent. Before June 10, 1991, the Block II correlator was not doing this correction properly [13].

The second error occurred in FIT. Instead of summing the correlator sine and cosine counts, FIT averaged the amplitudes over time and frequency; this resulted in too large an amplitude for observations with low SNR. This has been corrected. FIT now also makes a correction for a nonzero residual fringe rate.[9] FIT amplitudes are normalized with respect to the number of lags, the number of time points, and the number of frequency bins containing good data.

To verify the above calculations for correlated flux densities, a short baseline experiment was conducted. On a baseline of 500 m, the correlated flux densities of the compact extragalactic radio sources used for VLBI astrometry are almost the same (within 10 percent) as the total flux densities. Figure 1 is a plot of the experiment's final visibilities (S_{cor}/S_{total}) versus scan number. Fitting a constant to the visibilities gave a ratio of 0.92. This suggests one or more of the following: The sources are all partially resolved, the antenna gains used in the data analysis are too high, the system temperatures are too low, or the b-factor is too large. However, the chi-square of a fit to unity is only 0.72, so changing the b-factor or antenna gain models is unjustified. *If the sources are resolved by a few percent on average, as expected, the* b*-factor is accurate to about 5 percent.*

[9] S. C. Unwin, "Amplitude Errors in AIPS Global Fringe-Fitting," Caltech Interoffice Memorandum (internal document), California Institute of Technology, Pasadena, California, October 26, 1988.

B. System Temperatures

The power meter program, QMVLBI, has a zenith system temperature calibration procedure, as described above. The calibration is performed at the start of an experiment. As time passes, the accuracy of the calibration degrades due to weather changes and receiver gain variations. The receiver gain was checked for variability over a 24-hour experiment and was found to be extremely stable (less than 1-percent variance in the power-to-temperature conversion factor). However, changes in the outside temperature over 24 hours can cause a significant (up to 5-percent) change in the zenith system temperature. Weather changes (such as a passing cloud) can cause a more substantial change in system temperature at low elevations; these are measured by the power meter.

The power meters measure power across the entire high electron mobility transistor (HEMT) bandwidth (400 MHz at X-band and 100 MHz at S-band). The 14 recorded 2-MHz channels (which are not contiguous) are scattered throughout this range. Therefore, any radio interference falling outside the observed channels (but within the HEMT bandwidth) will cause a spuriously high system temperature reading. In the next version of station software, it will be possible to take system temperature measurements for each channel,[10] thereby eliminating this potentially serious problem. Until then, it is assumed that variations in system temperature (as well as receiver gain) across an entire band are negligible.

System temperature measurements using the power meters, the strip charts, and results from modeling all agree within the expected errors. Figure 2 is an example of temperature versus air mass for each observation for an experiment with measurements by all three methods. Note that even in the absence of any station system temperature measurements during an experiment, models can be used to get system temperatures that agree with the power meter values to about 20 percent.

On- and off-source system temperature measurements are estimated in a somewhat subjective fashion. For strong sources, inspection of the power meter data clearly reveals when the antenna gets on source and when it moves off. The magnitudes of the observed sharp rise and fall of the system temperature values are used to estimate the antenna temperature (that part of the system temperature due to the source). For the case of weak sources, it is not always possible to determine the antenna temperature. In addition, the error in antenna temperature is

[10] *DSN Systems Requirements*, Document 820-13, Module VLB-13-5, Jet Propulsion Laboratory, Pasadena, California, 1990.

difficult to determine since the bulk of the error in system temperature is not statistical in nature. Repeatability suggests an error of about 15 percent in antenna temperature (down to the detection limit of 0.1 K). Note that variations in antenna temperature across the 400-MHz bandwidth spanned by the wideband amplifier at X-band due to a nonzero spectral index will be less than 3 percent for a typical VLBI source. Also, the next version of station software will be able to take power data with finer time and power resolution than the present power meters; this will lower the error in total flux density for weak sources.

C. Antenna Pointing and Gain

Total flux density measurements are determined only from antenna temperature and antenna gain. Therefore, using a strong source (so as to minimize antenna temperature errors) with a known total flux density, it is possible to estimate the antenna gain. Some observations of the Very Large Array (VLA) calibrator source 3C 286 were used to compare the modeled antenna gains with gains estimated in this fashion. The resulting total flux densities were consistent at the 20-percent level.

An error in antenna pointing will yield reduced antenna temperatures and correlation amplitudes, giving spuriously low values of both total and correlated flux densities. Reference frame experiments use blind pointing; pointing correction tables, squint corrections, and refraction correction calculations are estimated to yield a blind pointing accuracy of ~10 mdeg for the 34-m antennas.[11] The refraction correction model used at the antennas was verified to agree, to within 1 mdeg, with refraction calculations using real-time meteorological parameters.[12] However, under similar circumstances (observations of the same source closely spaced in time and at approximately the same elevation, system temperature, and IHA), different X-band observations are seen to produce different correlated flux densities, sometimes by as much as a factor of 2. This is probably due to pointing errors; a pointing error of 30 mdeg by one station will reduce that antenna's X-band gain by ~50 percent (S-band gain is much less affected by pointing errors of this magnitude). This in turn yields a correlated flux density that is ~30 percent too small. The cause of this pointing problem is as yet unknown.

[11] D. Girdner, personal communication, Antenna Performance Engineer, TDA Mission Support and DSN Operations Section, February 15, 1992.

[12] G. E. Lanyi, "Atmospheric Refraction Corrections to Antenna Pointing at 1 Millidegree Accuracy," JPL Interoffice Memorandum 335.3-89-026 (internal document), Jet Propulsion Laboratory, Pasadena, California, March 24, 1989.

D. Comparison of Results With a Known Structure

The source 4C 39.25 has been a fairly well-studied source at high frequencies (see, for example, [14]). It is known to be extended in the east–west direction with knots in its structure. At X-band it is also highly time-variable [15]. Therefore, X-band correlated flux densities on two baselines on a monthly basis can give little source structure detail; indeed, it is found that measurements vary by more than a factor of 2 from month to month. The picture at S-band is much clearer; Fig. 3 is a plot of measured correlated flux density versus the projected east–west baseline length. The smoothness of the curve implies a smooth underlying source structure (to the limit of the resolution of the interferometer) and little time variability. The fact that the correlated flux density depends solely on the absolute value of the east–west projected baseline length suggests that the source is not resolved in the north–south direction. This is completely consistent with maps of 4C 39.25 that are in the literature.

IV. Error Budget

The variance, σ^2, in measured correlated flux density (for $\rho\pi/2 \ll 1$), derived from Eq. (1), is:

$$\sigma^2 = {S_{cor}}^2 \left(\frac{{\sigma_\rho}^2}{\rho^2} + \frac{{\sigma_b}^2}{b^2} + \frac{{\sigma_{T_1}}^2}{4\,{T_1}^2} + \frac{{\sigma_{T_2}}^2}{4\,{T_2}^2} + \frac{{\sigma_{G_1}}^2}{4\,{G_1}^2} + \frac{{\sigma_{G_2}}^2}{4\,{G_2}^2} \right) \quad (9)$$

where T_i is the system temperature for an observation at station i and G_i is the antenna gain for station i. Note that the error is proportional to the correlated flux density.

The total error in correlated flux density comes from a number of sources. Principal sources are the errors in the determination of system temperatures (about 5 percent when using the power meters), errors in gain due to weather and frequency variations within an experiment (about 5 percent), errors in ρ (typically less than 2 percent, determined by the SNR of the observation), and errors in b (approximately 5 percent).

A summary of total estimated errors from all sources, assuming uncorrelated errors as shown in Eq. (9), is given in Table 2. Note that in addition to the errors listed, time and structure variability can, in extreme cases, cause up to a factor of 2 error in correlated flux density values extrapolated from measurements at previous epochs.

V. Summary

With the methods described here, it is possible to provide correlated and total flux density measurements accurate to ~20 percent. This accuracy is sufficient to determine which antennas are necessary to observe a given source on a given baseline at a given time. A complete correlated and total flux density catalog can now be built. However, to get better than 20-percent accuracy, the pointing problems of the DSN antennas must be corrected.

Acknowledgments

Dave Fort was of great help in explaining the Block II correlator. Steve Lowe assisted with many discussions on correlated amplitudes. Roger Linfield provided invaluable comments and critiques.

References

[1] O. J. Sovers, C. D. Edwards, C. S. Jacobs, G. E. Lanyi, K. M. Liewer, and R. N. Treuhaft, "Astrometric Results of 1978–1985 Deep Space Network Radio Interferometry: The JPL 1987-1 Extragalactic Source Catalog," *Astron. J.*, vol. 95, pp. 1647–1658, 1988.

[2] R. N. Treuhaft and S. T. Lowe, "A Nanoradian Differential VLBI Tracking Demonstration," *TDA Progress Report 42-109*, vol. January–March 1992, Jet Propulsion Laboratory, Pasadena, California, pp. 1–15, May 15, 1992.

[3] T. F. Haddock, H. D. Aller, and M. F. Aller, "Frequent Observations of Extragalactic Compact Sources at 24 GHz," *Astron. J.*, vol. 93, pp. 1356–1367, June 10, 1987.

[4] A. E. Rogers and T. A. Clark, *Mark III Data Acquisition Terminal,* Crustal Dynamics Project, Goddard Space Flight Center, Greenbelt, Maryland, January 1982.

[5] J. S. Ulvestad and R. P. Linfield, "The Search for Reference Sources for ΔVLBI Navigation of the Galileo Spacecraft," *TDA Progress Report 42-84*, vol. October–December 1985, Jet Propulsion Laboratory, Pasadena, California, pp. 152–163, February 15, 1986.

[6] A. R. Thompson, J. M. Moran, and G. W. Swenson, Jr., *Interferometry and Synthesis in Radio Astronomy,* New York: John Wiley and Sons, pp. 10, 88, 248, and 305, 1986.

[7] S. T. Lowe, *Theory of Post Block II VLBI Observable Extraction,* JPL Publication 92-7, Jet Propulsion Laboratory, Pasadena, California, July 15, 1992.

[8] P. H. Richter and S. D. Slobin, "DSN 70-Meter Antenna X- and S-Band Calibration Part I: Gain Measurements," *TDA Progress Report 42-97*, vol. January–March 1989, Jet Propulsion Laboratory, Pasadena, California, pp. 314–346, May 15, 1989.

[9] S. D. Slobin and P. H. Richter, "DSN 70-Meter Antenna X- and S-Band Calibration Part II: System Noise Temperature Measurements and Telecommunications Link Evaluation," *TDA Progress Report 42-97*, vol. January–March 1989, Jet Propulsion Laboratory, Pasadena, California, pp. 352–366, May 15, 1989.

[10] C. C. Chao, *The Tropospheric Calibration Model for Mariner Mars 1971*, Technical Report 32-1587, Jet Propulsion Laboratory, Pasadena, California, pp. 61–76, March 1974.

[11] J. B. Thomas, *Interferometry Theory for the Block II Processor*, JPL Publication 87-29, Jet Propulsion Laboratory, Pasadena, California, October 15, 1987.

[12] M. L. Meeks, ed., *Methods of Experimental Physics*, vol. 12, Part C, Astrophysics, Radio Observations, New York: Academic Press, 1989.

[13] S. C. Unwin, ed., *JPL/Caltech Block II VLBI Correlator Newsletter*, vol. 2, no. 3, California Institute of Technology, Pasadena, California, July 1991.

[14] D. Shaffer and A. Marscher, "4C 39.25: Superluminal Motion Between Stationary Components," in *Superluminal Radio Sources*, edited by J. A. Zensus and T. J. Pearson, New York: Cambridge University Press, pp. 67–71, 1987.

[15] J. M. Marcaide, A. Alberdi, P. Elosegui, A. P. Marscher, Y. F. Zhang, D. B. Shaffer, C. J. Schalinski, A. Witzel, N. Jackson, and G. Sandell, "Detection of a New Component in the Peculiar Superluminal Quasar 4C 39.25," in *Parsec-scale Radio Jets: Proceedings of a Workshop Held at the National Radio Astronomy Observatory, Socorro, New Mexico, October 17–18, 1989*, edited by J. A. Zensus and T. J. Pearson, New York: Cambridge University Press, pp. 59–65, 1990.

Table 1. *b*-factor bandpass parameters for the Block II correlator.

	Mark III				Mark II			
	8 lags		16 lags		8 lags		16 lags	
	Empirical	Theory	Empirical	Theory	Empirical	Theory	Empirical	Theory
B^2 for bin 1	0.840	0.899	0.830	0.889	–	0.907	1.050	0.892
bin 2	1.002	1.002	0.992	1.015	–	0.993	1.122	1.015
bin 3	1.023	0.997	0.987	0.994	–	1.019	1.020	0.994
bin 4	0.643	0.604	1.003	1.003	–	0.523	1.004	1.004
bin 5	–	–	1.011	0.997	–	–	0.978	0.996
bin 6	–	–	1.001	0.977	–	–	0.935	0.999
bin 7	–	–	0.877	0.813	–	–	0.913	0.804
bin 8	–	–	0.467	0.408	–	–	0.337	0.244
D_N	0.877	0.876	0.896	0.887	–	0.871	0.921	0.869

Notes:

B^2 and D_N are relative to a square bandpass of amplitude unity.

No S- or X-band Mark II 8-lag data were available for analysis.

In 8-lag mode, bins 5 through 8 contain no signal.

Empirical fits were made relative to bin 2 (for 8 lags) or bin 4 (16 lags).

Mark II theoretical calculations based on an 11-pole Butterworth filter.

Table 2. Error sources.

Error source	Resulting fractional error, percent	
	X-band	S-band
Gain (each station)		
Weather and modeling	5	5
Pointing errors	0 to 50	0 to 10
b-factor	5	5
Amplitudes		
Signal to noise	0 to 15	0 to 15
FIT approximations	5	5
System temperatures (each station)		
Using model	10 to 15	15 to 20
Using strip chart	10	15
Using power meters	5	10
Estimated total (using power meters with T_{zen} at both stations)		
Clear weather, high elevation, high SNR source	10	10
Poor weather, low elevation, low SNR source	30	20

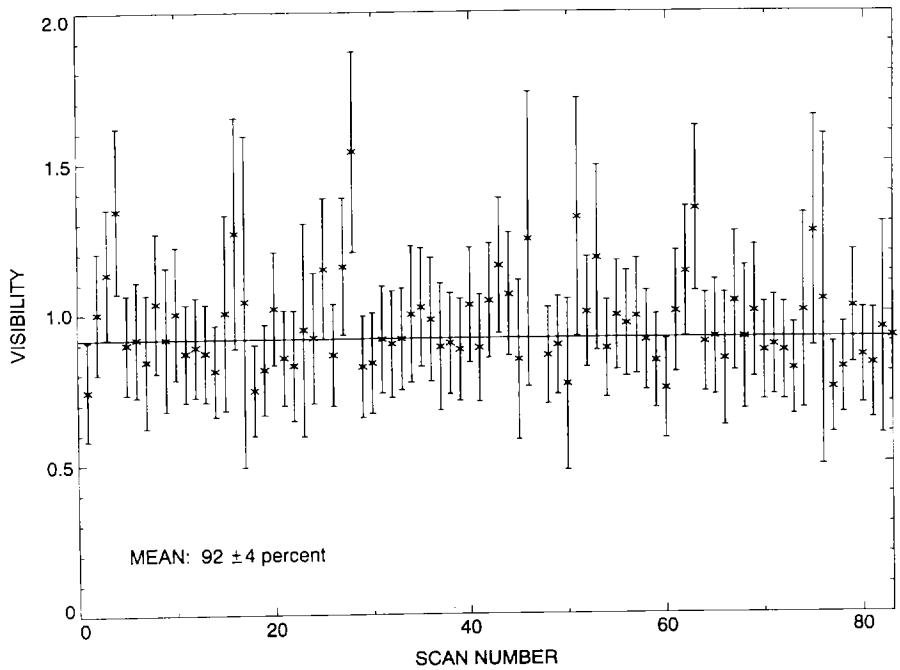

Fig. 1. The final visibilities (S_{cor}/S_{total}) for the short-baseline experiment 92CC124 using DSS 14 and DSS 15. The values for the total flux density, S_{total}, were taken from antenna temperature measurements at DSS 15. A weighted fit of zero slope was made to the data. The error bars are calculated from each observation's error in total flux density and in correlated flux density. For some scans, the antenna temperature was comparable to the resolution limit of 0.1 K; hence the large error bars.

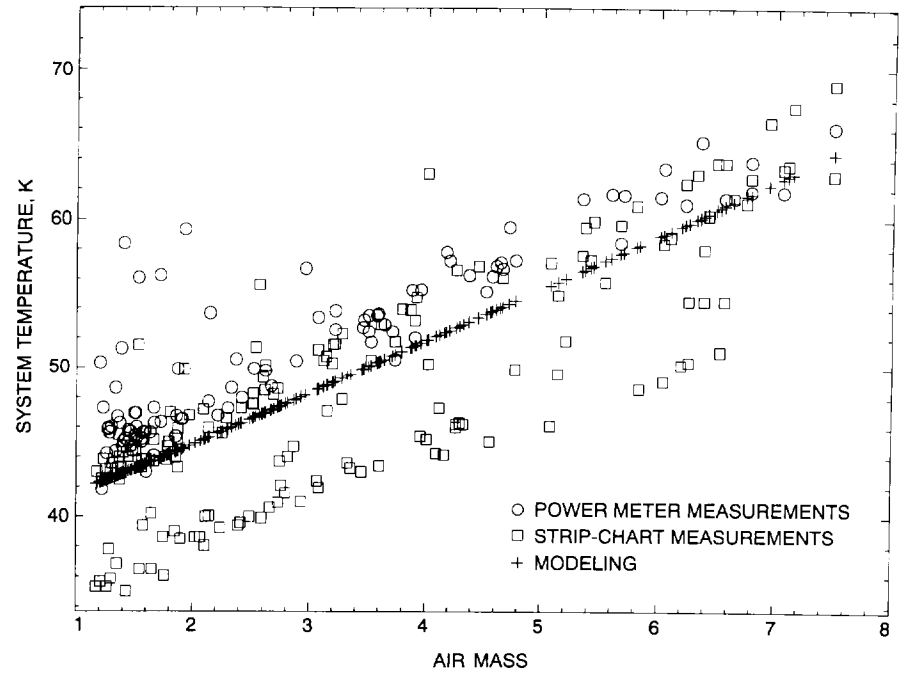

Fig. 2. A plot of X-band (8.4-GHz) system temperature versus air mass (1/sin (elevation)) for the three different methods for the experiment 90CA049. In most cases, agreement of the model with the power meter data is within 20 percent. The strip-chart data show an unexplained (and probably unreal) drop in system temperature halfway through the experiment.

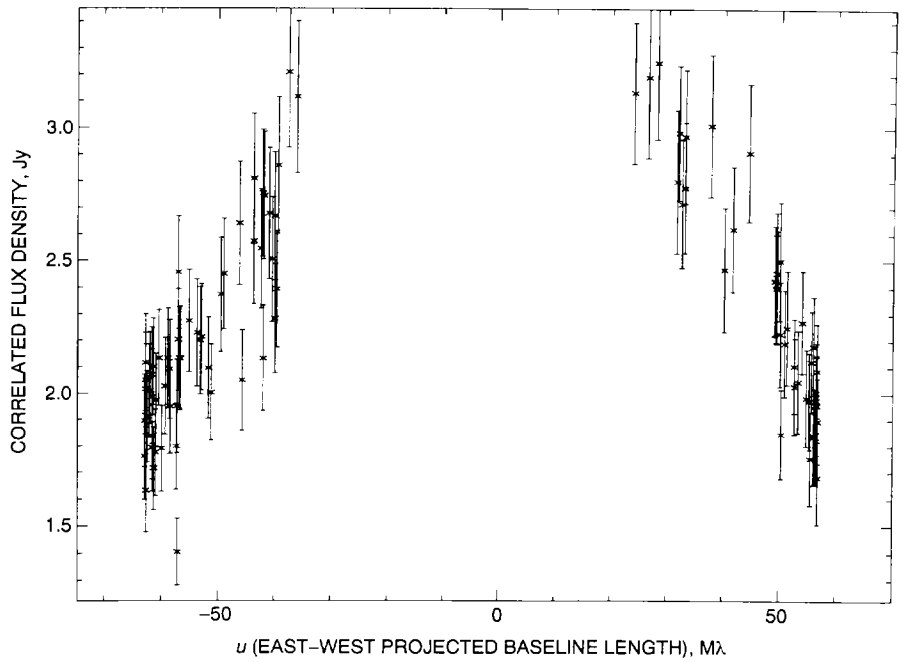

Fig. 3. A plot of correlated flux density versus *u* for the source 4C 39.25 at 2.3 GHz. The smoothness of the curve suggests smooth source structure. The dependence of correlated flux density solely on the absolute value of *u* suggests that the source is not resolved in the north–south direction but that it is extended in the east–west direction.